An integrated control-oriented modelling for HVAC performance benchmarking

Satyavada, Harish; Baldi, Simone

DOI
10.1016/j.jobe.2016.04.005

Publication date
2016

Document Version
Accepted author manuscript

Published in
Journal of Building Engineering

Link to formal publication Journal of Building Engineering (Elsevier): http://doi.org/10.1016/j.jobe.2016.04.005

An integrated control-oriented modelling for HVAC performance benchmarking

Simone Baldi and Harish Satyavada *
Delft Center for Systems and Control
Delft University of Technology,
Mekelweg 2 (3mE building),
2628 CD, Delft, The Netherlands.
Tel.: +31 15 2781823
s.baldi@tudelft.nl, h.satyavada@student.tudelft.nl

April 27, 2016

Abstract

Energy efficiency in building heating, ventilating and air conditioning (HVAC) equipment requires the development of accurate models for testing HVAC control strategies and corresponding energy consumption. In order to make the HVAC control synthesis computationally affordable, such control-oriented models are typically a simplified version of more elaborate building simulation environments (e.g. EnergyPlus, Modelica, TRNSYS). Despite their simplicity, control-oriented models must effectively catch all the interactions between HVAC equipment, in order achieve system integration and avoid fragmentation in HVAC modelling and control synthesis, which is one of the main causes of suboptimal performance in the building sector. In this work we propose an integrated control-oriented modelling for HVAC performance benchmarking. The following HVAC equipment and their interaction are modelled: condensing boiler, radiator, air handling unit, heat pump, chiller, fan, pump, pipe, duct, and multiple thermal zones. The proposed modelling approach is modular so that the user can add and remove as many components as desired, depending on the building to be modelled. Appropriate procedures for synthesis of control strategies and benchmarking are proposed. Extensive simulations demonstrate the effectiveness of the

proposed methodology, which can lead to improvements in occupants' thermal comfort while at the same time consistently attaining energy savings.
Keywords: HVAC modelling and control, HVAC system integration, energy efficiency.

1 Introduction

Heating, Ventilation and Air Conditioning (HVAC) systems, widely used in residential and commercial buildings, are responsible for a large part of the energy consumption worldwide. According to the estimates published by the U.S. Energy Information Administration and by the European Commission in 2014, more than 40% of total U.S. and Europe energy consumption was consumed in residential and commercial buildings, half of which was used for HVAC operation [1, 2]. It has been widely recognized that in order to enable energy efficiency in HVAC equipment it is crucial to develop accurate models for testing HVAC control strategies and their relative energy consumption [3, 4]. Nowadays, there is plenty of software tools used for building energy simulation purposes, among which EnergyPlus [5], Dymola-Modelica [6], TRNSYS [7]. These tools are very precious for energy simulation purposes, but they give limited insight on how to actually design HVAC control strategies for minimization of HVAC energy consumption. To this purpose, simpler models, often referred to as control-oriented models, need to be developed so as to make use of the rigorous tools of systems and control theory [8]. In order to make the control synthesis computationally affordable, such control-oriented models are typically a simplified version of the more elaborate building simulation environments EnergyPlus, Dymola-Modelica and TRNSYS. Despite their simplicity, control-oriented models must effectively catch all the interactions between HVAC equipment, in order to have an integrated environment and avoid fragmentation in HVAC modelling and control, which is often the first source of suboptimal performance in the building sector [9]. This fragmentation implies that control strategies are developed without accounting for possible HVAC component interactions, thus resulting in suboptimal energy performance. A typical example is control of air handling units (AHUs) for heating purposes [10]: the temperature of a room is not only affected by the heating coil used to regulate the temperature of the inlet air, but also by a radiator system. Both the heating coil and the radiator might be driven by the same boiler. As a result, control must carefully integrate these components by taking into account their interaction.

In order to better illustrate this fragmentation, let us look at the state of the art and industrial practice in HVAC modelling and control: unfortunately, HVAC interactions are often neglected. Components are often modelled separately, as illustrated by this overview on recent implementations of modelling and control strategies for HVAC systems: a chiller alone [11], a radiator alone [12], an AHU alone [13, 14, 15], a heat pump alone [16], AHUs with multiple zones [17, 18, 19], floor heating with multiple zones [20]. Some efforts toward HVAC integration can be recognized in works such as [21] (chiller and AHU), [22, 23] (AHU with chiller, fans and multiple zones), [24] (boiler, heat pump and chiller), even if many other HVAC components are still not integrated. This overview shows that HVAC system-wide control integration is far from being reached. In this work we aim at covering this gap by proposing an integrated control-oriented modelling for HVAC performance benchmarking. The following HVAC equipment (and their interaction) is modelled: condensing boilers, radiators, air handling units, heat pumps, chillers, fans, pumps, pipes, ducts, and thermal zones. The proposed modelling approach is modular so that the user can add and remove as many HVAC components as desired, depending on the building to be modelled.

Modelling is only the first step toward HVAC system integration: in fact, the final goal is HVAC energy efficiency via improved controls. To this purpose, the second step is the selection of the HVAC control parameters in an optimal way. In this work we finally overcome the aforementioned HVAC fragmentation by exploiting the proposed modelling approach to synthesize and evaluate integrated HVAC control strategies. In particular, after adopting a control architecture commonly used in the building sector (a lower proportional-integral-derivative control layer, and an upper optimization-based control layer to optimize the lower layer operation), we exploit the proposed modelling approach to find the optimal working points of the HVAC equipment, to auto-tune a set of feedback control strategies, and to develop appropriate benchmarking criteria. Extensive simulations demonstrate the effectiveness of the proposed methodology, which can lead to improvements in occupants' thermal comfort while at the same time consistently attaining energy savings.

The rest of the paper is organized as follows: Section 2 describes the modelling of the HVAC equipment. Partial differential equations are derived, which are then spatially discretized in Section 3 so as to obtain a control oriented modelling of the HVAC system. Section 4 illustrates the functioning of the model, while Section 5 presents the proposed methods for parameter identification and controller synthesis. Section 6 verifies the effectiveness of the methods via simulation and Section 7 concludes the paper.

2 Modelling the HVAC components

This section presents the heat and mass transfer equations governing a complete HVAC system consisting of condensing boilers, radiators, air handling units (with heating and cooling coils), heat pumps, chillers, fans, pumps, pipes, ducts and thermal zones. Interaction between components are also modelled, e.g. the heating coil is connected to a (condensing) boiler, while the cooling coil to a chiller. The boiler heats supply water, which is circulated throughout the system and aids in warming the zone through the radiator and also by interacting with the air through the heating coil in the AHU. A heat pump is finally connected to the floor heating system of the house. Lumped capacitance models are chosen for radiator, boiler, pipes, ducts and heating coil, resulting in partial differential equations which are spatially discretized so as to come up with control-oriented models. Fig. 1 shows a possible integration of all the components into a building: where a thermal zone is heated by floor heating connected to a heat pump, a boiler which is connected to both a radiator and an air handling unit. The air handling unit uses a heating coil (connected to the boiler) and a cooling coil (connected to a chiller) to warm or cool the air. Pumps and fans are used to put water and air in motion. Fig. 1 is just a possible example of HVAC configuration. The user can add and remove HVAC components depending on the building to be modelled. Additional thermal zones and floors can also been added.

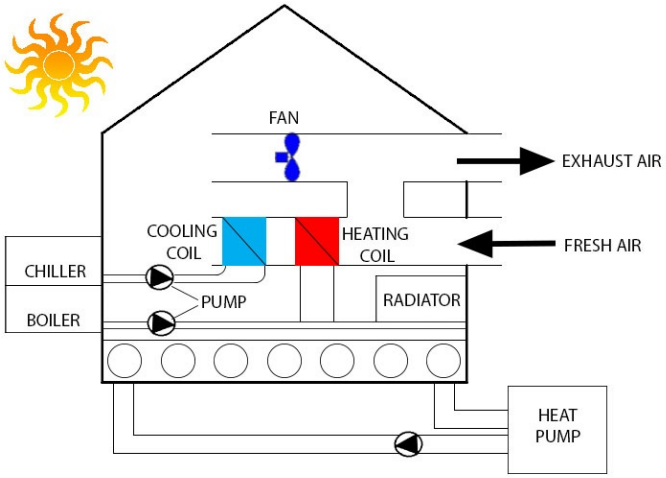

Figure 1: Overview of the main components of the HVAC system

2.1 Radiator

A simplifying assumption is made in the model of the radiator [12], assuming the same temperature for radiator surface as the water temperature inside the radiator. By this assumption, the heat from the radiator is transferred to the ambient only by convection. The indoor air in the zone acts as an ambient for the radiator. The evolution of radiator temperature T_{rad} in [^{o}C] is as follows:

$$\frac{\partial T_{rad}}{\partial t} = \frac{w_{rad_{sw}}}{\rho_w A_{rad}} \frac{\partial T_{rad}}{\partial l} - \frac{K_{rad}}{C_w \rho_w V_{rad}} (T_{rad} - T_z), \tag{1}$$

where the first term represents heat exchange inside the radiator and the second term represents the heat exchange with the indoor air temperature T_z in [^{o}C] of the zone. In (1) C_w is the thermal capacitance of water in [kJ/kg^{o}C], $w_{rad_{sw}}$ is the mass flow rate of supply water into the radiator in [kg/s], K_{rad} is the heat transfer coefficient in [kW/^{o}C], ρ_w is the water density in [kg/m^3], A_{rad} is the surface area of the radiator in [m^2] and V_{rad} is the volume of the radiator in [m^3]. The heat transfer coefficient K_{rad} is described as:

$$K_{rad} = h_{rad} A_{rad}, \tag{2}$$

where h_{rad} is the convection heat transfer coefficient of the radiator in [kW/m^2 ^{o}C]. The power transferred, Q_{rad} in [kW] by the radiator to the zone is given by the following equation:

$$Q_{rad} = K_{rad} (T_{rad} - T_z). \tag{3}$$

2.2 Condensing boiler

In most countries, it is now a requirement of the building regulations that newly installed gas-fired boilers should be condensing with a seasonal efficiency of 85% or more [25]. Since the exit flue gas temperature of a conventional gas fired boiler is usually high and a great amount of heat energy is lost to the environment, condensing boilers aim at recovering both sensible heat and latent heat by adding a condensing heat exchanger. The evolution of water temperature inside the boiler T_b in [^{o}C] is as follows:

$$\frac{\partial T_b}{\partial t} = \frac{w_{b_{sw}}}{\rho_w A_b} \frac{\partial T_b}{\partial l} + \frac{Q_b(T_{b_{rw}}, P^b_{in})}{C_w \rho_w V_b}, \tag{4}$$

where the first term represents heat exchange inside the boiler. In (4) Q_b is the power supplied by the boiler in [kW], $w_{b_{sw}}$ is the mass flow rate of supply water into the boiler in [kg/s], A_b is the surface area of the boiler in [m^2] and V_b is the volume of the boiler in [m^3]. As shown in details in Section 3, the power supplied by the boiler Q_b is modelled as a polynomial function of the return water $T_{b_{rw}}$ in [^{o}C] and of the supplied fuel P_{in}^b in [kW] (e.g. natural gas).

2.3 Heat pump

The heat pump is assumed to be connected to the floor heating. It takes the return water from the floor heating circuit and it supplies water at a higher temperature. The evolution of water temperature inside the heat pump T_{hp} in [^{o}C] is as follows:

$$\frac{\partial T_{hp}}{\partial t} = \frac{w_{hp_{sw}}}{\rho_w A_{hp}} \frac{\partial T_{hp}}{\partial l} + \frac{Q_{hp}(T_{hp_{rw}}, T_{amb}, f_{hp})}{C_w \rho_w V_{hp}}, \tag{5}$$

where the first term represents heat exchange inside the heat pump. In (5) Q_{hp} is the power supplied by the heat pump in [kW], $w_{hp_{sw}}$ is the mass flow rate of supply water into the heat pump in [kg/s], A_{hp} is the surface area of the heat pump in [m^2] and V_{hp} is the volume of the heat pump in [m^3]. As shown in details in Section 3, the power supplied by the heat pump Q_{hp} is modelled as a polynomial function of the return water $T_{hp_{rw}}$ in [^{o}C], ambient temperature T_{amb} in [^{o}C] and compressor frequency f_{hp} in [H].

2.4 Chiller

The chiller can be thought as the counterpart of a heat pump. It use energy to chill the return water and supplies it at a lower temperature. The chiller is connected to the cooling coil of the AHU. The evolution of water temperature inside the chiller T_c in [^{o}C] is as follows:

$$\frac{\partial T_c}{\partial t} = \frac{w_{c_{sw}}}{\rho_w A_c} \frac{\partial T_c}{\partial l} - \frac{Q_c(T_{c_{rw}}, T_{amb}, f_c)}{C_w \rho_w V_c}, \tag{6}$$

where the first term represents heat exchange inside the chiller. In (6) Q_c is the power supplied by the chiller in [kW], $w_{c_{sw}}$ is the mass flow rate of supply water into the chiller in [kg/s], A_c is the surface area of the chiller in [m^2] and V_c is the volume of the chiller in [m^3]. Similarly to the heat pump, as shown in details in Section 3, the power supplied by the chiller Q_c is modelled as a polynomial

function of the return water $T_{c_{rw}}$ in [^{o}C], ambient temperature T_{amb} in [^{o}C] and compressor frequency f_c in [H].

2.5 Pipes and ducts

Pipes (resp. ducts) transport water (resp. air) across various components in the HVAC system. An assumption is made that the pipe's (duct's) surface temperature is the same as the water (air) temperature inside the pipe (duct). In the system under consideration all the pipes (ducts) are located inside the building envelope. As a result, the ambient temperature for the pipes (ducts) is the envelope temperature. The evolution of a pipe temperature T_p in [^{o}C] is as follows:

$$\frac{\partial T_p}{\partial t} = \frac{w_w}{\rho_w A_p}\frac{\partial T_p}{\partial l} - \frac{K_r}{C_w \rho_w V_p}(T_p - T_{wall}), \tag{7}$$

where the first term represents heat exchange inside the pipe and the second term represents heat exchange with the wall temperature T_{wall} in [^{o}C]. In (7) w_w is the mass flow rate of water in the pipe in [kg/s], K_r is the heat transfer coefficient in [kW/^{o}C], A_p is the surface area of the pipe in [m^2] and V_p is the volume of the pipe in [m^3]. The heat transfer coefficient K_r can be described as:

$$K_r = h_r \pi D_p L_p, \tag{8}$$

where h_r is the convection heat transfer coefficient of the pipe in [kW/m^2 ^{o}C], D_p is the diameter of the pipe in [m] and L_p is the length of the pipe in [m]. Similar equations can be derived for the ducts, taking care of substituting pipe temperature T_p with duct temperature T_d, volume of the pipe V_p with volume of the duct V_d etc.

2.6 Heating and cooling coils

The heating and cooling coils are sub-components of the AHU. For example, in the heating coil, the air from mixing zone interacts with the hot water. The result of this interaction can be modelled with the following equations:

$$\frac{\partial T_{hc_a}}{\partial t} = \frac{w_{hc_a}}{\rho_a A_d}\frac{\partial T_{hc_a}}{\partial l} - \frac{K_{rd}}{C_a \rho_a V_d}(T_{hc_a} - T_{hc_w}). \tag{9}$$

$$\frac{\partial T_{hc_w}}{\partial t} = \frac{w_{hc_w}}{\rho_w A_p}\frac{\partial T_{hc_w}}{\partial l} - \frac{K_r}{C_w \rho_w V_p}(T_{hc_w} - T_{hc_a}). \tag{10}$$

In (9) evolution of temperature of air in the duct in heating coil T_{hc_a} in [^{o}C] as a result of heat exchange inside the duct present in the heating coil as given by the first term and heat exchange with the water temperature T_{hc_w} in [^{o}C] as given by the second term, is described. In (9) w_{hc_a} is the mass flow rate of air in the duct in heating coil in [kg/s]. In (10) evolution of temperature of water in the pipe in heating coil T_{hc_w} in [^{o}C] as a result of heat exchange inside the pipe as given by the first term and heat exchange with the air temperature T_{hc_a} in [^{o}C] as given by the second term, is described. In (10) w_{hc_w} is the mass flow rate of water in the pipe in the heating coil in [kg/s]. Similar equations can be derived for the cooling coil, paying attention to substitute the temperature of air in the duct in heating coil T_{hc_a} with the temperature of air in the duct in cooling coil T_{cc_a}, the mass flow rate w_{hc_w} of water in the pipe in the heating coil with the mass flow rate w_{cc_w} of water in the pipe in the cooling coil, etc.

2.7 Valve and Splitter

The supply water is divided into two (or more) flows at the splitter. Let us assume that one flow goes to the heating coil in AHU and the other to the radiator (even though different connections can be modelled). The valve dictates the mass flow rate of water in each of the flows. The valve opening $\tilde{c}(t)$ is given by the following equation [8]:

$$\tilde{c}(t) = \frac{c(t)}{\sqrt{(c^2(t)(1-N_v)+N_v)}}. \tag{11}$$

In (11) $c(t)$ is the control signal and N_v is the valve authority. Typically $c(t) \in [0,1]$. The mass flow rate of water flowing into the heating coil in AHU is given by:

$$w_{hc_w} = \tilde{c} w_{b_{sw}}.$$

Mass flow rate of water flowing into the radiator is given by:

$$w_{rad_{sw}} = w_{b_{sw}} - w_{hc_w}.$$

2.8 Collector

The collector is a counterpart of the splitter. The collector accumulates water flows from the radiator and the AHU. Due to merging of these two flows, the resulting

mass flow rate changes as follows:

$$w_{b_{sw}} = w_{hc_w} + w_{rad_{sw}}.$$

The temperature of the mixture T_{mix} in [^{o}C] is given by the following equation:

$$T_{mix} = \frac{w_{hc_w} T_{hc_{rw}} + w_{rad_{sw}} T_{rad_{rw}}}{w_{b_{sw}}}, \tag{12}$$

where $T_{hc_{rw}}$ is the temperature of return water from the heating coil in [^{o}C] and $T_{rad_{rw}}$ is the temperature of return water from the radiator in [^{o}C].

2.9 Pump

Pumps control flow rate of water through the HVAC system as described by:

$$w_{b_{sw}} = v_w A_p \rho_w,$$

where v_w is the velocity of water flow in [m/s]. The temperature of water passing through the pump increases due to the inefficiencies of the pump motor if the motor is installed in the water stream [8]. The increase in temperature is given by the following equation:

$$T_{po_{rw}} = T_{pi_{rw}} + \frac{W_p f}{w_{b_{sw}} C_w}, \tag{13}$$

where $T_{po_{rw}}$ is the return water temperature at the pump outlet in [^{o}C], $T_{pi_{rw}}$ is the return water temperature at the pump inlet in [^{o}C], W_p is the power consumed by pump in [kW] and f is a fraction of the pump power converted into fluid thermal energy.

2.10 Mixing zone

The mixing zone is a sub-component of the AHU. As a result of interaction between fresh air and return air through the recirculating damper, there is a change in the mass flow rate and temperature of the mixture. The dynamics of the interaction are similar to that of a collector and are given by the following equations:

$$w_{mix_{sa}} = w_{f_a} + w_{r_a}, \tag{14}$$

$$T_{mix_{sa}} = \frac{w_{f_a} T_{f_a} + w_{r_a} T_{r_a}}{w_{mix_{sa}}}. \tag{15}$$

In (14) $w_{mix_{sa}}$ is the mass flow rate of the mixture in [kg/s], w_{f_a} is the mass flow rate of fresh air in [kg/s] and w_{r_a} is the mass flow rate of return air in [kg/s]. In (15) $T_{mix_{sa}}$ is the temperature of the mixture in [^{o}C], T_{f_a} is the temperature of fresh air entering the mixing zone in [^{o}C] and T_{r_a} is the temperature of return air through the recirculating damper entering the mixing zone in [^{o}C].

2.11 Fan

Analogous to the pump, the fan determines the flow rate of the air through the AHU as described by:

$$w_{mix_{sa}} = \rho_a v_a A_d,$$

where v_a is the velocity of air flow in [m/s]. The temperature of air passing through the fan increases due to the inefficiencies of the fan motor if the motor is installed in the air stream. The increase in temperature is given by the following equation:

$$T_{fo_{sa}} = T_{fi_{sa}} + \frac{W_f f_a}{w_{mix_{sa}} C_w}, \tag{16}$$

where $T_{fo_{sa}}$ is the supply air temperature at the fan outlet in [^{o}C], $T_{fi_{sa}}$ is the supply air temperature at the fan inlet in [^{o}C], W_f is the power consumed by the fan in [kW] and f_a is a fraction of the fan power converted into fluid thermal energy.

2.12 Damper

In this model, a recirculating air damper is considered. The recirculating damper controls the percentage mix of the return and fresh air. The mass flow-rate of air w_{r_a} in [kg/s] leaving the recirculating damper is given by the following equations [26]:

$$\alpha_r = (1 - pd)(\alpha_0 - 90) + 90, \tag{17}$$

$$G_{dr} = e^{\frac{b(\alpha_0 - \alpha_r)}{2}}, \tag{18}$$

$$N_{dr} = \frac{\Delta P_{dr}}{(P_{se} + P_{sf} + \Delta P_{dr})}, \tag{19}$$

$$G'_{dr} = G_{dr}\left[G_{dr}^2(1 - N_{dr}) + N_{dr}\right], \tag{20}$$

$$w_{r_a} = G'_{dr} w_{o_{ra}}. \tag{21}$$

In (17) α_r represents recirculating damper blade position, α_0 is a value between 0° and 10° and pd is control signal to the damper ($0 \leq pd \leq 1$). In (18) G_{dr} is a damper inherent characteristic and b is an empirical constant which depends on the damper blade profile, number of blades and blade action. Typically $0.075 < b < 0.11$. In (19) N_{dr} represents damper authority, ΔP_{dr} represents pressure drop across the damper in [Pa], P_{se} represents static pressure at discharge in [Pa] and P_{sf} represents static pressure at the inlet in [Pa]. G'_{dr} in (20) is an installed characteristic which determines the amount of the return air passing through the recirculating damper. Typically G'_{dr} is a value between 0 and 1. In (21) $w_{o_{ra}}$ is the mass flow rate of air entering the damper in [kg/s].

2.13 Zone

In this model of the zone all walls, ceiling and glazing are assumed to have the same characteristics which are grouped together as envelop parameters [12]. The evolution of wall temperature T_{wall} in [^{o}C] is as follows:

$$\frac{dT_{wall}}{dt} = \frac{U_{wo}A_{wall}(T_{o_a} - T_{wall})}{C_{wall}} + \frac{U_{wi}A_{wall}(T_z - T_{wall})}{C_{wall}} + \frac{U_{wo}A_{wall}(T_{z_{neigh}} - T_{wall})}{C_{wall}} + \frac{(1-p)Q_s}{C_{wall}}, \tag{22}$$

where the first term represents the heat exchange with outside air temperature T_{o_a} in [^{o}C], the second term represents the heat exchange with the zone indoor air temperature T_z in [^{o}C] and the third term represents the heat exchange with the neighbor zone indoor air temperature $T_{z_{neigh}}$ in [^{o}C]. Notice that interaction with multiple zones can be included in (22) by opportunely choosing the surface area A_{wall} through which the different zones interact. In (22) U_{wo} and U_{wi} are the thermal transmittances of outer and inner layers of the wall respectively in [kW/m^2 ^{o}C], C_{wall} is thermal capacitance of wall in [kJ/kg^{o}C], A_{wall} is the surface area of the wall in [m^2], p is a fraction of solar radiation through glazing and Q_s is solar radiation in [kW]. Two separate temperature layers for the floor are considered to make the model extendable to the situation where floor heating is available as another heat source. The evolution of the first layer of floor temperature T_{f_1} in [^{o}C] is as follows:

$$\frac{dT_{f_1}}{dt} = \frac{h_{ri}A_f(T_z - T_{f_1}) + U_{f_1}A_f(T_{f_2} - T_{f_1}) + pQ_s}{C_{f_1}}, \tag{23}$$

where the first term represents the heat exchange with indoor air temperature of the zone and the second term represents the heat exchange with the second layer floor temperature T_{f_2} in [^{o}C]. In (23) h_{ri} is the convection heat transfer coefficient of the indoor air in [kW/m^2 ^{o}C], U_{f_1} is the thermal transmittance of first layer of floor in [kW/m^2 ^{o}C], C_{f_1} is the thermal capacitance of the first layer of floor in [kJ/kg ^{o}C] and A_f is the surface area of the floor in [m^2]. The evolution of the second layer of floor temperature T_{f_2} in [^{o}C] is as follows:

$$\frac{dT_{f_2}}{dt} = \frac{U_{f_1}A_f(T_{f_1} - T_{f_2}) + U_{f_2}A_f(T_g - T_{f_2}) + Q_f}{C_{f_2}}, \tag{24}$$

where the first term represents the heat exchange with the first layer of the floor and the second term represents the heat exchange with ground temperature T_g in [^{o}C]. In (24) U_{f_2} is the thermal transmittance of second layer of floor in [kW/m^2 ^oC], C_{f_2} is the thermal capacitance of the second layer of the floor in [kJ/kg ^{o}C] and Q_f is the heat supplied by the floor heating in [kW]. Notice that the second layer of floor can be the ceiling of a lower floor: in such case (24) can be modified as:

$$\frac{dT_{f_2}}{dt} = \frac{U_{f_1}A_f(T_{f_1} - T_{f_2}) + U_{f_2}A_f(T_{z_{LOW}} - T_{f_2}) + Q_f}{C_{f_2}}, \tag{25}$$

where $T_{z_{LOW}}$ in [^{o}C] is the temperature of the zone at the lower floor. In this way it is possible to modularily include multi-floor buildings. The evolution of indoor air temperature of the zone is as follows:

$$\begin{aligned}\frac{dT_z}{dt} = \frac{U_{wi}A_{wall}}{C_r}(T_{wall} - T_z) + \frac{h_{ri}A_f}{C_r}(T_{f_1} - T_z) + \frac{U_{f_2}A_f}{C_r}(T_{f_{2_{UP}}} - T_z) \\ + \frac{C_a w_{mix_{sa}}}{C_r}(T_{ahu_{sa}} - T_z) + \frac{Q_{rad}}{C_r} + \frac{Q_e}{C_r},\end{aligned} \tag{26}$$

where the first term represents the heat exchange with the wall temperature, the second term represents the heat exchange with the first layer floor temperature and third term represents the heat exchange with the ceiling ($T_{f_{2_{UP}}}$ is the temperature of the second layer of the upper floor). The fourth term represents the heat exchange with the air temperature $T_{ahu_{sa}}$ in [^{o}C] entering the zone from the AHU. In (26) Q_e is internal heat gains in [kW]. In fact, the zone temperature is also dependent on occupancy, internal gains and their schedule, all taken into account by Q_e. Of course this contribution needs to be measured or estimated somehow, why is not always obvious. In our approach we followed the EnergyPlus strategy of estimating the average power of equipment inside the thermal zone (PC, appliances), and estimate the average heat gain per person (130 W).

3 Control Oriented Modelling

The partial differential equations of the lumped capacitance models of the radiator, boiler, heat pump, chiller, pipes, ducts and heating/cooling coils are spatially discretized to obtain a model suitable for simulation and control. Lumped models can be spatially discretized into N elements. Temperature in every element T_n for $n \in 1,2 \ldots N$ can be modelled as a separate state. The state of each one of these elements represents the temperature of water or air in that particular element. Backward discretization in space has been used for the dicretization of these models [26]: as an example we show the discretized the radiator model:

$$\frac{dT_{\phi_x}}{dt} = \frac{C_w w_{rad_{sw}}}{C_w \rho_w A_{rad} \Delta l}(T_{\phi_{x-1}} - T_{\phi_x}) - \frac{K_{rad}}{C_w \rho_w V_{rad}}(T_{\phi_x} - T_z), \tag{27}$$

where T_{ϕ_x} in [^{o}C] is the state T_{rad} corresponding to the water temperature in the radiator, $T_{\phi_{x-1}}$ in [^{o}C] is the water inlet temperature at the radiator and Δl is the length of the element in [m]. Fig. 2 shows the main idea behind spatial discretization of partial differential equations. The equations of boiler, heat pump, chiller, pipes, ducts and heating/cooling coils are discretized in a similar fashion. All the resulting equations can be easily implemented in MATLAB and customized according to the HVAC topology that ones desires to model. Furthermore, by increasing the number N of discretization elements one can obtain finely discretized models (with many states, typically used for simulation purposes) or coarsely discretized models (with less states, typically used for control purposes).

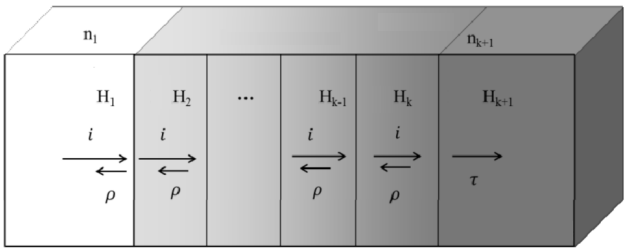

Figure 2: Backward discretization of partial differential equations

3.1 Power calculation

It is common practice to model the power consumed by HVAC equipment via polynomial functions [5]. For the condensing boiler case we have

$$Q_b = \eta_b(P^b_{in}, T_{b_{rw}})P^b_{in}, \tag{28}$$

where $P^b_{in} = H_v v_g$ is the boiler input power (v_g is the gas volumetric flow and H_v is the gas heating value for volume), and η_b is the boiler efficiency curve, described by

$$\begin{aligned}\eta_b(P^b_{in}, T_{b_{rw}}) &= a^b_0 + a^b_1 T_{b_{rw}} + a^b_2 T^2_{b_{rw}} + a^b_3 T^3_{b_{rw}} + a^b_4 T^4_{b_{rw}} \\ &\quad + a^b_5 P^b_{in} + a^b_6 T_{b_{rw}} P^b_{in} + a^b_7 T^2_{b_{rw}} P^b_{in},\end{aligned} \tag{29}$$

for some appropriate coefficients to be identified. In a similar way for the heat pump we have

$$Q_{hp} = \eta_{hp}(T_{hp_{rw}}, f_{hp}, T_{amb})P^{hp}_{in}, \tag{30}$$

where P^{hp}_{in} is heat pump input power (typically electric), and η_{hp} is the boiler efficiency curve, described by

$$\begin{aligned}\eta_{hp}(T_{hp_{rw}}, f_{hp}, T_{amb}) &= a^{hp}_0 + a^{hp}_1 T_{amb} + a^{hp}_2 T_{hp_{rw}} + a^{hp}_3 f_{hp} + a^{hp}_4 T^2_{amb} + a^{hp}_5 T^2_{hp_{rw}} \\ &\quad + a^{hp}_6 f^2_{hp} + a^{hp}_7 T_{amb} T_{hp_{rw}} + a^{hp}_8 T_{amb} f_{hp} + a^{hp}_9 T_{hp_{rw}} f_{hp},\end{aligned} \tag{31}$$

for some appropriate coefficients to be identified. Similarly for the chiller

$$\begin{aligned}\eta_c(T_{c_{rw}}, f_c, T_{amb}) &= a^c_0 + a^c_1 T_{amb} + a^c_2 T_{c_{rw}} + a^c_3 f_c + a^c_4 T^2_{amb} + a^c_5 T^2_{c_{rw}} \\ &\quad + a^c_6 f^2_c + a^c_7 T_{amb} T_{c_{rw}} + a^c_8 T_{amb} f_c + a^c_9 T_{c_{rw}} f_c\end{aligned} \tag{32}$$

Fig. 3 shows the polynomial efficiency curves for this HVAC equipment. To calculate the hydraulic power consumed by the pump while rotating at a certain velocity q_w, we use the following formula [27]:

$$W_p = \frac{q_w \rho_w g h}{3.6 \cdot 10^6}, \tag{33}$$

where W_p represents power consumed by the pump in [kW], q_w represents flow capacity in [m^3/h], g represents acceleration due to gravity in [m/s^2] and h represents differential head in [m]. To calculate the power consumed by the fan W_f

in [kW] to circulate air in the AHU at a certain velocity q_a, we use the following formula [28]:

$$W_f = \frac{\Delta P q_a}{1.0 \cdot 10^3}, \tag{34}$$

where ΔP is total pressure increase in the fan in [Pa], q_a represents air volume flow delivered by the fan in [m^3/s].

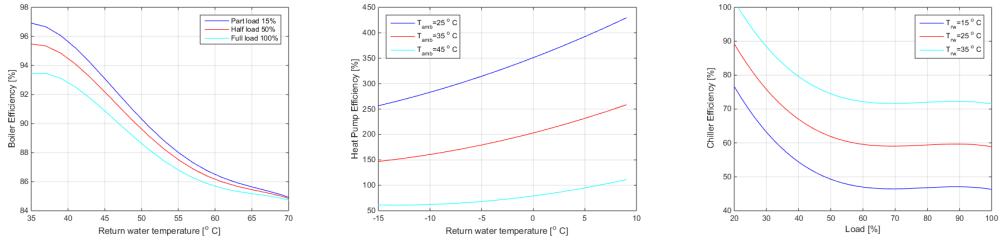

(a) Boiler efficiency (b) Heat pump efficiency (c) Chiller efficiency

Figure 3: Boiler, heat pump and chiller efficiency curves

4 Functioning of the model

In order to illustrate the functioning of the model, we will isolate a few components and highlight their effect on the zone temperature. For the sake of conciseness, we will deal with the radiator and the AHU.

4.1 Highlighting the functioning of the radiator

In order to highlight the functioning of the radiator alone, the valve is operated in such a way that that almost all the water flowed through the radiator and very less to the AHU. Also the mass flow rate of air was made almost zero so that there is not much air through the AHU and consequently the AHU contribution of heat to the room is negligible.
It is expected that the temperature of the zone increases when the boiler is on. As long as the boiler is on, hot water flows into the radiator and it transfers heat into the zone. When the boiler is cut off, the zone temperature should decrease, as there is no heat transfer from the radiator (boiler cut off) and the AHU (already made sure almost no air flows through the AHU).

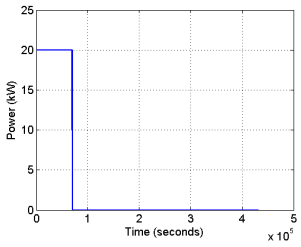

(a) Heat transferred by the boiler

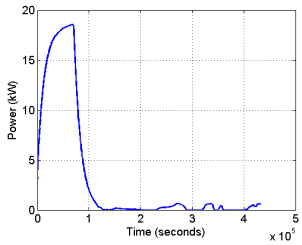

(b) Heat transferred by the radiator

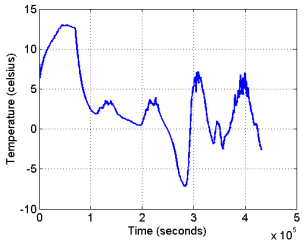

(c) Zone temperature

Figure 4: Heat transferred by boiler, radiator and zone temperature evolution for five days

The simulation was run for 432000 seconds which translates to 5 days. To show the changes in zone temperature reflected by various phenomenon, the boiler was switched on at a power 20 kW for the first day (precisely 70000 s) after that the boiler was cut off the for the remaining four days. The heat transferred by boiler is shown in Fig. 4a. Fig. 4b shows that the radiator transfers heat to the zone as long as the boiler is on. Fig. 4 shows that the zone temperature increases in the first day and, once the boiler is off, the heat transferred by the radiator and the zone temperature decreases.

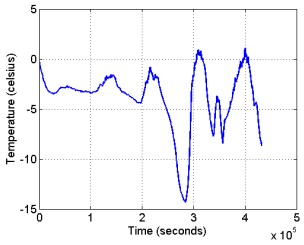

(a) Outside temperature

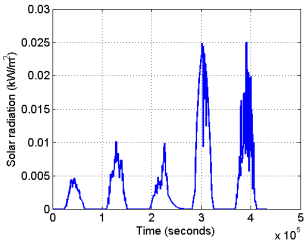

(b) Solar radiation profile

Figure 5: External weather conditions for the five days

The weather profile for five days (outside temperature and solar radiation) is shown in Fig. 5. It can be observed that in the night between the third and the fourth day the outside temperature is at its lowest. The solar radiation peaks correspond to the time of the day when the sun is shining the brightest. It can be observed that on the last two days, the sun shines the brightest. Going back to Fig. 4, we can observe that the initial temperature of the zone is around 6° C. The

temperature rises for the first day, when the boiler is on and the room is heated up to 13° C. This is a reasonable temperature considering the initial temperature, the limited power of the boiler and the fact that the outside temperature is negative and the solar radiation during the 1st day is also very low.

4.2 Highlighting the functioning of the AHU (heating)

In order to highlight the heating function of the AHU alone, the valve is operated in such a way that that almost all the hot water water flows through the AHU and very less to the radiator. It is expected that, as long as the boiler is on, hot water flows into the heating coil of the AHU, which warms up the air in the AHU. The hot air from AHU flows into the zone consequently warming up the zone.
The simulation was run for 432000 seconds which translates to five days. In order to highlight the changes in zone temperature reflected by various phenomenon, the boiler was switched on for the first day alone (precisely 70000 seconds) after that the boiler was cut off the for the remaining four days. The heat transferred by boiler is shown in Fig. 6a.
The value 15 kW was chosen noticing that the air handling unit takes in air from outside (fresh air). This fresh air first mixes with the warmer return air (air from zone). The mixed air gets heated in the heating coil and then flows through ducts into the zone. Fig. 6 shows the changes in temperature as the air flows through mixing zone and heating coil. It can be observed from Fig. 6c that the air in the mixing zone is heated up to 6.5° C. This is a reasonable value as the fresh air temperature is negative. As seen from Fig. 6d the air from the mixing zone is now further heated up to 10° C. Fig. 6e shows that as the mixed air flows though ducts into the zone, a slight drop in temperature occurs because of heat losses in ducts. Finally, the air from AHU interacts with zone air, which results in increase in temperature for the first day. The room is heated up to 10° C. This is a reasonable temperature considering that the outside temperature is negative and the solar radiation during the first day is very low. After the first day there is an obvious drop in temperature of the air profile in all the units as the boiler is off.

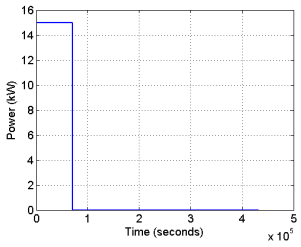

(a) Heat transferred by the boiler

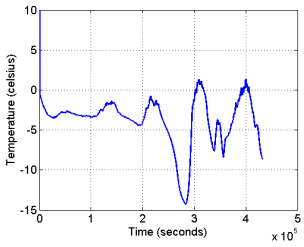

(b) Temperature of fresh air entering the AHU

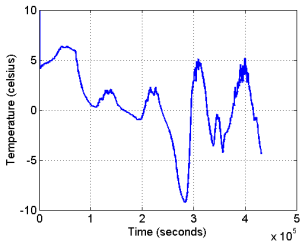

(c) Fresh air temperature after interacting with return air

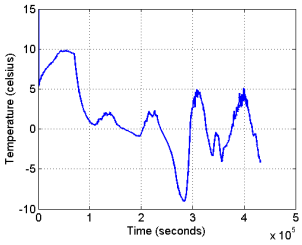

(d) Temperature of the air after getting warmed in the heating coil

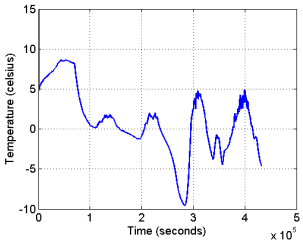

(e) Temperature of the air entering the zone from the AHU

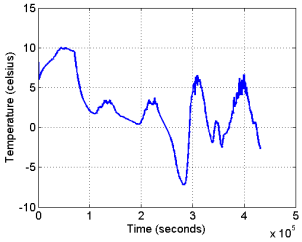

(f) Zone temperature

Figure 6: Heat transferred by boiler and air temperature profiles in different parts of the AHU

4.3 Highlighting the functioning of the AHU (cooling)

In order to highlight the cooling function of the AHU alone, the valve is operated in such a way that that almost all the cold water water flows through the AHU and very less to the radiator. It is expected that, as long as the chiller is on, cold water flows into the cooling coil of the AHU, which cools up the air in the AHU. The cold air from AHU flows into the zone consequently cooling up the zone.
The simulation was run for 432000 seconds which translates to five days. In order to highlight the changes in zone temperature reflected by various phenomenon, the chiller was switched on for the first day alone (precisely 70000 seconds) and after that the chiller was cut off the for the remaining four days. The heat transferred by chiller is shown in Fig. 7a.

The value 15 kW was chosen noticing that the air handling unit takes in air from outside (fresh air). This fresh air first mixes with the colder return air (air from zone). The mixed air gets cooled in the cooling coil and then flows through

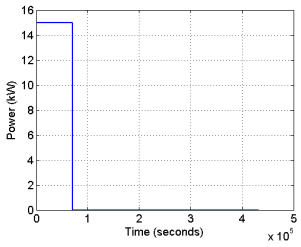

(a) Heat transferred by the chiller

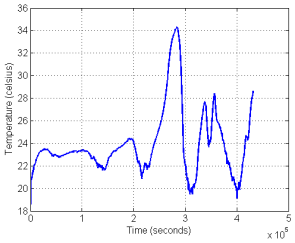

(b) Temperature of fresh air entering the AHU

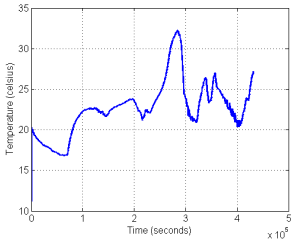

(c) Fresh air temperature after interacting with return air

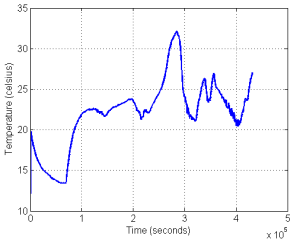

(d) Temperature of the air after getting cooled in the cooling coil

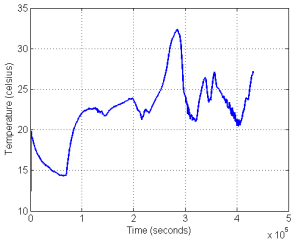

(e) Temperature of the air entering the zone from the AHU

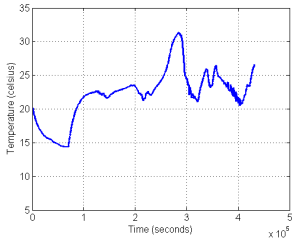

(f) Zone temperature

Figure 7: Heat transferred by chiller and air temperature profiles in different parts of the AHU

ducts into the zone. Fig. 7 shows the changes in temperature as the air flows through mixing zone and cooling coil. It can be observed from Fig. 7c that the air in the mixing zone is cooled up to 17° C. This is a reasonable value as the fresh air temperature is as high as 23.5° C. As seen from Fig. 7d the air from the mixing zone is now further cooled up to 14° C in the cooling coil. Fig. 7e shows that as the mixed air flows though ducts into the zone, a slight change in temperature occurs because of heat losses in ducts. Finally, the air from AHU interacts with zone air, which decreases the temperature for the first day. The room is cooled up to 14.8° C. This is a reasonable temperature considering that the outside temperature is high. After the first day there is an obvious increase in temperature of the air profile in all the units as the chiller is off.

5 Methods for parameter identification and controller synthesis

All the equations developed in Sections 2 and 3 can be aggregated together in an integrated HVAC model of the form

$$\dot{x}(t) = f(x(t), \theta) + g(x(t), u(t), d(t), \theta), \tag{35}$$

where $x \in \mathbb{R}^n$, represents all the states (temperatures at the different HVAC elements), $u \in \mathbb{R}^m$ represents the inputs to the system (powers or velocities at which run each HVAC component, and valves and dampers position) and $d \in \mathbb{R}^r$ represents the disturbances that act on the system (solar radiation, outside and ground temperature). In addition, the model depends on a set of parameters $\theta \in \mathbb{R}^p$ (heat transfer coefficients, coefficients of efficiency curves) which must be appropriately chosen. The determination of such coefficients passes through two steps:

- an *initial parameter guess* for such coefficients can be made based on knowledge of materials (e.g. envelope materials, pipe and ducts size and insulation characteristics) and HVAC components datasheets (for efficiency curves);

- using real-life data or data coming from more elaborate building simulation environments (e.g. EnergyPlus, Modelica, TRNSYS), one can use nonlinear identification techniques, like the levenberg-marquardt or the trust-region-reflective algorithms implement in Matlab [29], to find the *best parameters* that minimize the gap between the control-oriented model and the real-building;

Notice that an effective way to make the gap between the real building and its model as small as desired is to increase the complexity of the model by increasing the spatially discretized grid of the partial differential equations. This comes however at the expense of increasing the number of states and of parameters to be identified, which also complicates the controller synthesis. The user is thus requested to find the better trade-off between model fidelity and computational affordability of HVAC control strategy.

In order to find the parameters of our proposed model we consider a heating problem in one zone with a boiler, a radiator and an air handling unit (including pipes, ducts, fans and pumps). The zone has also been modelled in EnergyPlus

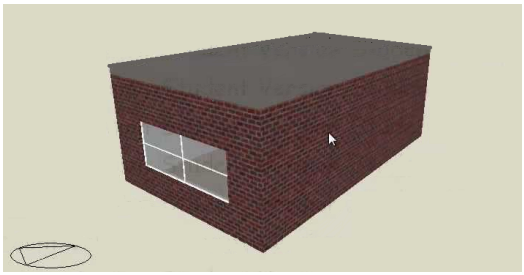

Figure 8: EnergyPlus one zone model

and it is shown in Fig. 8. The objective is to find the parameter of our model in such a way that the behavior of our model matches the one in EnergyPlus.

The following parameters are assumed to be known: physical properties of water and air, volume of boiler and radiator, area of floor and envelope. The following variables are assumed to be measured: solar radiation, temperature of outside air, mixing air, return air, return and supply water, water and air mass flow rate, input power to the boiler, pump and fan velocity. The following parameters need to be estimated: boiler efficiency curve, heat exchange coefficiects of floor, envelope, pipes and ducts. The purpose is to tune the unknown parameters of the proposed integrated model (INT) in such a way that the behavior (temperature and energy consumption) of the proposed model matches as close as possible the behavior of the EnergyPlus (EP) model. The following percentage cost is chosen

$$\lambda \frac{\sum_{t=1}^{T}(T_{z_{EP}}(t)-T_{z_{INT}}(t))^2}{\sum_{t=1}^{T}T_{z_{EP}}^2(t)}+(1-\lambda)\frac{\sum_{t=1}^{T}(Q_{HVAC_{EP}}(t)-Q_{HVAC_{INT}}(t))^2}{\sum_{t=1}^{T}Q_{HVAC_{EP}}^2(t)}, \quad (36)$$

which is solved for $\lambda = 0.5$ using Matlab [29]. Note that while the first temperature-related term in (36) can be useful to estimate the thermal parameters of envelope, pipes, ducts etc. the second energy-related term in (36) is particularly useful to tune all the parameters related to efficiency of boiler, heat-pump, chiller and other equipment (Q_{HVAC} sums up the energy consumptions of all the relevant HVAC equipment). The result of the estimation is a good match of the zone temperatures, as shown in Fig. 9. Table 1 shows that the gap between the EnergyPlus and the proposed model has been reduced from 15.8 % (for the model with initially guessed parameters) to 2.7 % (for the model with parameters optimized via identification). The energy consumption of the EnergyPlus model is compared with the energy consumption of the proposed integrated model in Fig.10. The comparison shows that the energy consumed by both the models is very much similar.

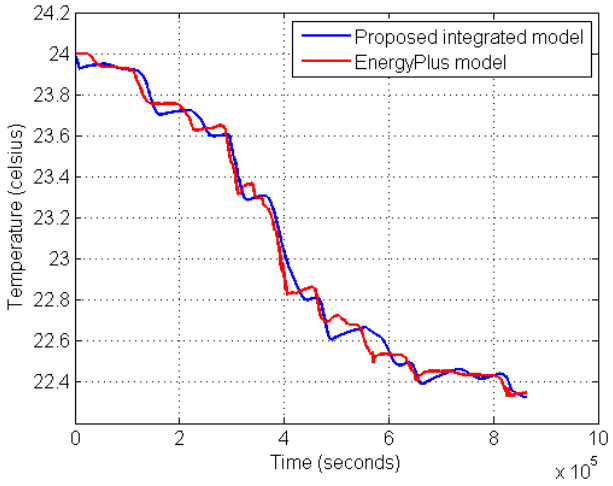

Figure 9: Matches between the zone temperature in the EnergyPlus model and in the proposed integrated model.

Table 1: Parameter identification performance: gap between EnergyPlus and proposed model before and after optimization

	Gap (%)
Initial model	15.8 %
Optimized model	2.7 %

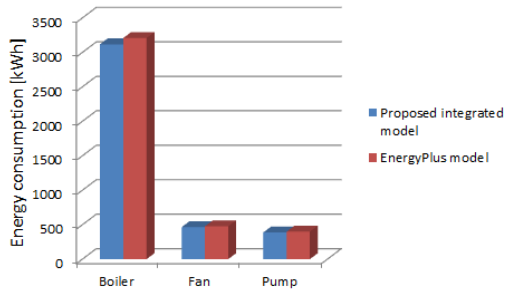

Figure 10: Comparison between the energy consumption of the EnergyPlus model and the proposed integrated model over a period of ten days.

Once a good control-oriented model has been obtained, the next step is designing HVAC control strategies. Nowadays huge research efforts are being invested in the development of Building Energy Management System (BEMS) which aims at automating the climate control problem by implementing optimal HVAC control strategies (and also provide feedback to the users or store thermal preferences) [3, 30, 31, 32]. Synthesis of HVAC control strategies passes through the definition of appropriate control objectives. A typical control objective is to maintain the zone temperature at a value guaranteeing desired comfort and indoor air quality, while at the same time minimizing energy consumption, e.g.

$$\sum_{t=1}^{T} (T_z(t) - T_{z_{des}}(t))^2 + \lambda (Q_{HVAC}(t))^2 \tag{37}$$

where the first term minimizes the deviation from a desired temperature, while the second term, weighted by a user-defined constant $\lambda > 0$, sums up the energy consumptions of all the relevant HVAC equipment. The quantity T stands for a simulation horizon over which we desire the cost to be minimized. At this point it is useful to introduce the two-level architecture shown in Fig. 11, typically used in the building sector:

- the *low-level control layer* is composed of proportional-integral-derivative (PID) controllers, one for each HVAC component, which are in charge of running the component at the operating point decided by the upper-level control layer, while tracking the desired temperature. In order to track the desired temperature, the PID layer can exploit the feedback between the desired and the actual temperature in the zone;

- the *upper-level control layer* is composed of advanced optimization-based controllers, which are in charge of deciding the operating points for each HVAC equipment (power and velocity) in such a way that the overall HVAC power consumption is minimized.

Typical techniques used for the lower layer include Ziegler-Nichols PID tuning or other more advanced automatic tuning strategies [33, 34]. For the upper layer it is common practice to resort to Model-based Predictive Controllers (MPC) [35, 36], rule-based strategies [37, 31, 38], planning via mixed integer programming and discrete optimization [39, 40] or other multiobjective optimization techniques [41, 42, 43]. In the following we will show how the proposed control-oriented modelling facilitates a more intuitive and easy to implement control architecture.

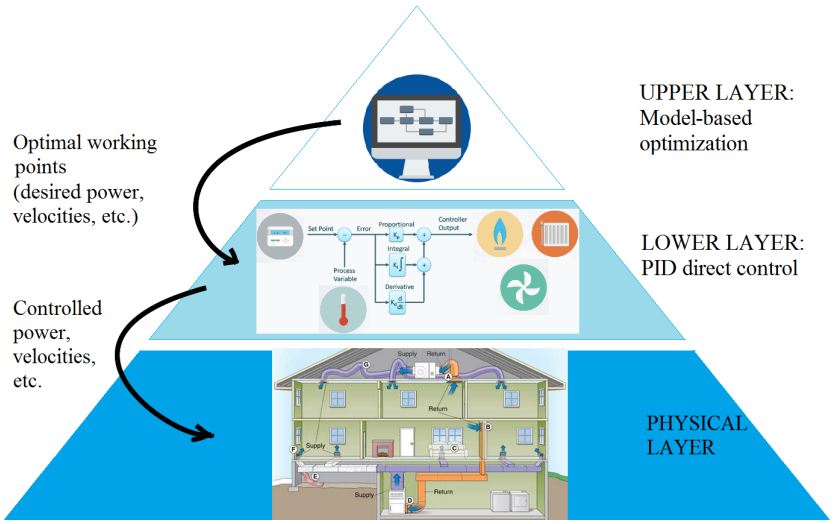

Figure 11: Two level architecture used in the building sector

5.1 Proposed low-level and upper-level control layers

We first notice that the integrated model (35) allows the solution of the following problem at every time t

$$0 = f(x_{eq}(t), \theta) + g(x_{eq}(t), u_{eq}(t), d(t), \theta), \tag{38}$$

where x_{eq} and u_{eq} represent the equilibrium states and inputs of the system at every time t (notice that the equilibria are dependent on the disturbances d acting on the system). Problem (38) can be solved at every time t, and if forecast for external weather conditions are available, over a control horizon in the future. Since an analytical expression for the functions f and g in (35) is available, problem (38) can be solved efficiently using a Newton-Raphson method [44]: in case multiple equilibria are present, one can even apply a constrained optimization to find the equilibria minimizing the integrated HVAC power consumption. In a similar way, comfort-related constraints can be added to make sure that the zone temperature will not violate certain bounds.

Once energy-efficient equilibria have been obtained, the low-level control layer can be implemented as follows:

$$u(t) = u_{eq}(t) + PID(s)(x(t) - x_{eq}(t)), \tag{39}$$

where $PID(s)$ is the transfer function of the PID controller, which can be written

as:

$$\begin{aligned} u(t) &= u_{eq}(t) + K_p(x(t) - x_{eq}(t)) + T_d x_d \\ &\quad + \int_0^t \left[K_i(x(\tau) - x_{eq}(\tau)) + K_b \left(sat(x(\tau) - x_{eq}(\tau)) - (x(\tau) - x_{eq}(\tau)) \right) \right] d\tau, \\ x_d(t) &= K_d(x(t) - x_{eq}(t)) - T_d \int_0^t x_d(t) d\tau, \end{aligned} \tag{40}$$

where the derivative action includes the time constant T_d of the first-order derivative filter. Furthermore, in (40) the back-calculation anti-windup method with constant K_b is enabled. This term is an internal tracking loop that discharges the integrator output [45]. Notice that (40) is a closed-loop feedback control that will add robustness with respect to model uncertainties. The PID controller can be tuned, in a simulation-based fashion using optimization techniques like interior-point and trust-region-reflective methods implemented in Matlab [46], in such a way to minimize the cost (37) or any other cost of interest.

Remark 1 *The availability of the analytical expression for the functions f and g in (35) allows to use gradient-based and hessian-based optimization, which can dramatically increase convergence speed. Note that the established tools for building energy simulation (EnergyPlus, TRNSYS, Modelica, etc) are very effective in evaluating energy consumption, but they generally fail in providing a general methodology for optimized controls. In fact, if control optimization is desired, the control designer will have to run extensive EnergyPlus, TRNSYS, Modelica simulations to calibrate the control parameters and check their effectiveness in terms of energy consumption [47]. The main advantage of the proposed approach is its equation-based nature, i.e. an analytical formula (35) is obtained for the heat/mass transfer processes. The result is that the control designer does not have to calibrate the control parameters by trial-and-error, but energy-minimizing controls can be found via very fast gradient/hessian-based optimization algorithms, e.g. the interior-point or and trust-region-reflective methods implemented in Matlab. Gradient and hessian can be calculated thanks to the availability of an analytical model. Note that the lack of an analytical model makes it impossible to use gradient/hessian-based optimization algorithms in EnergyPlus, TRNSYS, Modelica (the gradient needs to be estimated numerically, which requires several extra-simulations). Finally, the availability of an analytical model like in (35) makes gradient/hessian-based optimization scalable to even large buildings with multiple rooms and HVAC equipment.*

Remark 2 *The optimized controls that the proposed approach is able to calculate are position of valves and dampers, frequency of the fan/heat-pump/pump drive etc, i.e. low level controls, which can be directly implemented by a BEMS. This is in contrast with many approaches that can be found in literature (e.g. EnergyPlus, RC modelling, etc), where the low-level control layer cannot be reached and the control variable is directly the HVAC power, i.e. high level controls: this means that an extra control layer is necessary to translate such power into position of valves and dampers, frequency of the fan/heat-pump/pump drive etc. (operation which is not always easy, and which is typically done either in a decentralized (and thus suboptimal) way or adopting time expensive evolutionary algorithms [48, 30, 49, 14]). The proposed approach reaches directly the low level control layer, thus providing more useful information for the implementation of the control action in the BEMS.*

6 Simulations

In the following, extensive simulations are run on a test case which has been built via the proposed modelling approach. Parameter identification has been performed using `lsqnonlin` from Matlab, while two control strategies are benchmarked:

- a baseline PID strategy;
- a PID strategy optimized according to the cost (37);

In both cases, the upper-level control layer has been implemented by solving Problem (38) subject to comfort constraints and minimization of integrated HVAC power consumption. In Fig. 12 the gas consumed to operate the boiler and electricity consumed to operate the pump and fan by each of the two control strategies is shown. Also in Fig. 12 dissatisfaction percentage is listed. The dissatisfaction percentage has been calculated using the adaptive comfort model explained in the ASHRAE 55 standard [50]. According to the ASHRAE standard, a good thermal comfort is achieved when less than 10 % of the people are dissatisfied. It can be noticed from Fig. 12 that the proposed optimized PID strategy consistently satisfies the bound, while the baseline strategy is very close to or violates the bound.

Tables 2 and 3 show the gas and electricity consumed and dissatisfaction percentage for each of the control strategies over a simulation length of three and ten

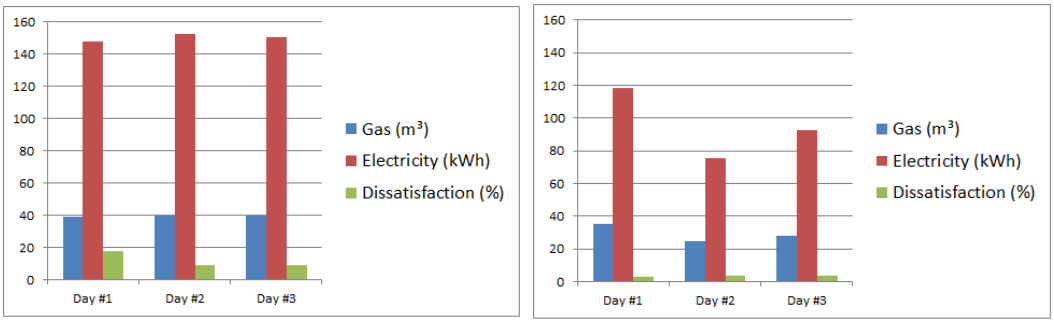

(a) Baseline PID strategy

(b) Optimal PID strategy

Figure 12: Gas, electricity consumed and thermal comfort dissatisfaction for each of the control strategies

days. Notice that the three days correspond to the three days used for the optimization routine, while the period of ten days has been used for validation purposes. The reduction in gas, electricity consumption and dissatisfaction percentage is also mentioned in the tables.

Table 2: Gas, electricity consumed and dissatisfaction percentage for a simulation length of three days

	Gas (m^3)	Electricity (kWh)	Dissatisfaction (%)
Baseline strategy	118.9	451.57	11.98
Optimal strategy	88.48	286.40	3.59
Reduction wrt Baseline	25.58%	36.58%	70.03%

Table 3: Gas, electricity consumed and dissatisfaction percentage for a simulation length of ten days

	Gas (m^3)	Electricity (kWh)	Dissatisfaction (%)
Baseline strategy	394.73	1492	15.76
Optimal strategy	283.39	850.86	4.56
Reduction wrt Baseline	28.20%	42.97%	71.06%

From Table 2 and Table 3 it is evident that the gas and electricity consumption and dissatisfaction percentage is minimized for the optimal PID strategy when compared to the baseline PID strategy for both the periods. In fact, the percentage of reduction, slightly increases in the validation period. It is remarkable that with the optimal PID strategy better comfort conditions are achieved while sensibly saving energy.

7 Conclusions and future work

We proposed a control-oriented modelling approach with the ability to effectively catch all the interactions between HVAC equipment. The following HVAC equipment was modelled: condensing boilers, radiators, air handling units, heat pumps, chillers, fans, pumps, pipes, ducts, and thermal zones. The proposed modelling approach has been shown to be modular so that the user can add and remove as many HVAC components as desired, depending on the building he desires to model. The proposed modelling thus allows the creation of an integrated environment for testing the energy performance of HVAC control strategies: in such a way, we proposed a framework to avoid fragmentation in HVAC modelling and control, which is often the first source of suboptimal performance in the building sector. Furthermore, we proposed appropriate procedures for parameter identification (in such a way that the model is as close as possible to elaborate building simulation environments like EnergyPlus, Modelica, TRNSYS, etc.) and synthesis of control strategies. Extensive simulations have demonstrated the effectiveness of the proposed methodology, which can lead to improvements in occupants' thermal comfort while at the same time consistently attaining energy savings. Future work will include augmenting the potentialities of the proposed modelling. Relevant directions are modelling gas emissions like carbon monoxide (CO), carbon dioxide (CO_2) and mono-nitrogen oxides (NO_x) emissions. In addition, it is interesting to explore the possibility to use control-oriented models for designing model-based fault detection and diagnosis techniques that could detect, isolate and identify possible faults in different HVAC components. Finally, future work will include increasing the confidence in the proposed methodology by developing a fully-fledged software certified via standards like BESTEST (ANSI/ASHRAE Standard 140-2011).

References

[1] U.S. Energy Information Administration. *Residential Energy Consumption Survey (RECS) and Commercial Buildings Energy Consumption Survey (CBECS)*. (EIA), 2014.

[2] Ian Knight. Assessing electrical energy use in hvac systems. `http://www.rehva.eu/fileadmin/hvac-dictio/01-2012/assessing-electrical-energy-use-in-hvac-systems_rj1201.pdf`, 2012.

[3] H.S. Sane, C. Haugstetter, and S.A. Bortoff. Building hvac control systems - role of controls and optimization. *2006 American Control Conference*, 2006.

[4] I. Knight. Why energy monitoring and feedback is essential to achieve sustained energy efficiency in eu buildings. *REHVA European HVAC Journal*, 51:16–19, 2014.

[5] U. S Department of Energy. Energyplus energy simulation software. `http://apps1.eere.energy.gov/buildings/energyplus/`, 2016.

[6] Lawrence Berkeley National Laboratory. Modelica library for building energy and control systems. `https://simulationresearch.lbl.gov/modelica`, 2016.

[7] SA Klein. *TRNSYS: A transient simulation program*. 2016.

[8] A. Afram and F. Janabi-Sharifi. Review of modeling methods for hvac systems. *Applied Thermal Engineering*, 67:507–519, 2014.

[9] Working Group III Report Intergovernmental Panel on Climate Change (IPCC). *Climate Change 2014: Mitigation of Climate Change*. IPCC Fifth Assessment Report, 2014.

[10] Y. Yu, D. Woradechjumroen, and D. Yu. A review of fault detection and diagnosis methodologies on air handling units. *Energy and Buildings*, 82:550–562, 2014.

[11] Marco Bonvini, Michael D. Sohn, Jessica Granderson, Michael Wetter, and Mary Ann Piette. Robust on-line fault detection diagnosis for hvac components based on nonlinear state estimation techniques. *Applied Energy*, 124:156–166, 2014.

[12] Fatemeh Tahersima, Jakob Stoustrup, Henrik Rasmussen, Peter Gammeljord Nielsen. Thermal analysis of an hvac system with trv controlled hydronic radiator. Toronto, ON, 2010. IEEE Conference on Automation Science and Engineering (CASE), IEEE.

[13] John M. House, Theodore F. Smith. Optimal control of building and hvac systems. seattle, washington, 1995. Proceedings of the American Control Conference, IEEE.

[14] Muhammad Waqas Khan, Mohammad Ahmad Choudhry, Muhammad Zeeshan, Ahsan Ali. Adaptive fuzzy multivariable controller design based on genetic algorithm for an air handling unit. *Energy*, pages 1–12, 2014.

[15] Chengyi Guo, Qing Song and Wenjian Cai. A neural network assisted cascade control system for air handling unit. *Industrial Electronics, IEEE Transactions on*, 54(1):620–627, 2007.

[16] Clara Verhelst, Filip Logist, Jan Van Impe, and Lieve Helsen. Study of the optimal control problem formulation for modulating air-to-water heat pumps connected to a residential floor heating system. *Energy and Buildings*, 45:43–53, 2012.

[17] SajidHussain b, HossamA.Gabbar, DanielBondarenko, FarayiMusharavati, ShaligramPokhare. Comfort-based fuzzy control optimization for energy conservation in hvac systems. *Applied Thermal Engineering*, 67:507–519, 2014.

[18] S. Baldi, A. Karagevrekis, I. Michailidis, and E. B. Kosmatopoulos. Joint energy demand and thermal comfort optimization in photovoltaic-equipped interconnected microgrids. *Energy Conversion and Management*, 101:352–363, 2015.

[19] C. D. Korkas, S. Baldi, I. Michailidis, and E. B. Kosmatopoulos. Intelligent energy and thermal comfort management in grid-connected microgrids with heterogeneous occupancy schedule. *Applied Energy*, 149:194–203, 2015.

[20] I. Michailidis, S. Baldi, M. F. Pichler, E. B. Kosmatopoulos, and J. R. Santiago. Proactive control for solar energy exploitation: A german high-inertia building case study. *Applied Energy*, 155:409–420, 2015.

[21] M. Schicktanz, T. Nunez. Modelling of an adsorption chiller for dynamic system simulation. *International Journal of Refrigeration*, 32(4):588–595, 2009.

[22] M Mossolly, K Ghali, and N Ghaddar. Optimal control strategy for a multi-zone air conditioning system using a genetic algorithm. *Energy*, 34(1):58–66, 2009.

[23] EH Mathews, DC Arndt, CB Piani, and E Van Heerden. Developing cost efficient control strategies to ensure optimal energy use and sufficient indoor comfort. *Applied Energy*, 66(2):135–159, 2000.

[24] M. Bojica and S. Dragicevic. Milp optimization of energy supply by using a boiler, a condensing turbine and a heat pump. *Energy Conversion and Management*, 43:591–608, 2002.

[25] *ClearFire Condensing Boiler Operation, Service, and Parts*. Cleaver Brooks, 2015.

[26] C. P. Underwood and F. W. H. Yik. *Modelling Methods for Energy in Buildings*. Blackwell Publishing Ltd, 2004.

[27] The Engineering Toolbox. Pumps - power calculator. `http://www.engineeringtoolbox.com/pumps-power-d_505.html`.

[28] The Engineering Toolbox. Fans - efficiency and power consumption. `http://www.engineeringtoolbox.com/fans-efficiency-power-consumption-d_197.html`.

[29] Mathworks. lsqnonlin. `http://en.mathworks.com/help/optim/ug/lsqnonlin.html`, 2016.

[30] S. Wang, Z. Ma. Supervisory and optimal control of building hvac systems: a review. *HVAC and R Research*, 14:3–32, 2008.

[31] Xiaoqi Xu, Patricia J Culligan, and John E Taylor. Energy saving alignment strategy: achieving energy efficiency in urban buildings by matching occupant temperature preferences with a buildings indoor thermal environment. *Applied Energy*, 123:209–219, 2014.

[32] S. Baldi, I. Michailidis, C. Ravanis, and E. B. Kosmatopoulos. Model-based and model-free "plug-and-play" building energy efficient control. *Applied Energy*, 154:829–841, 2015.

[33] Zhu Wang, Rui Yang, Lingfeng Wang, RC Green, and Anastasios I Dounis. A fuzzy adaptive comfort temperature model with grey predictor for multi-agent control system of smart building. In *Evolutionary Computation (CEC), 2011 IEEE Congress on*, pages 728–735. IEEE, 2011.

[34] C Tzivanidis, KA Antonopoulos, and F Gioti. Numerical simulation of cooling energy consumption in connection with thermostat operation mode and comfort requirements for the athens buildings. *Applied Energy*, 88(8):2871–2884, 2011.

[35] Truong X Nghiem and George J Pappas. Receding-horizon supervisory control of green buildings. In *American Control Conference (ACC), 2011*, pages 4416–4421. IEEE, 2011.

[36] A. Parisio, E. Rikos, G. Tzamalis, and L. Glielmo. Use of model predictive control for experimental microgrid optimization. *Applied Energy*, 115:37–46, 2014.

[37] I. Michailidis, S. Baldi, E. B. Kosmatopoulos, and Y. S. Boutalis. Optimization-based active techniques for energy efficient building control part ii: Real-life experimental results. *International conference on buildings energy efficiency and renewable energy sources, BEE RES*, pages 39–42, 2014.

[38] Gabriele Comodi, Andrea Giantomassi, Marco Severini, Stefano Squartini, Francesco Ferracuti, Alessandro Fonti, Davide Nardi Cesarini, Matteo Morodo, and Fabio Polonara. Multi-apartment residential microgrid with electrical and thermal storage devices: Experimental analysis and simulation of energy management strategies. *Applied Energy*, 137:854–866, 2015.

[39] M. Marzband, A. Sumper, A. Ruiz-Alvarez, J. L. Dominguez-Garcia, and B. Tomoiaga. Experimental evaluation of a real time energy management system for stand-alone microgrids in day-ahead markets. *Applied Energy*, 106:365–376, 2013.

[40] G. M. Kopanos, M. C. Georgiadis, and E. N. Pistikopoulos. Energy production planning of a network of micro combined heat and power generators. *Applied Energy*, 102:1522–1534, 2013.

[41] Kenichi Tanaka, Akihiro Yoza, Kazuki Ogimi, Atsushi Yona, Tomonobu Senjyu, Toshihisa Funabashi, and Chul-Hwan Kim. Optimal operation of dc smart house system by controllable loads based on smart grid topology. *Renewable Energy*, 39(1):132–139, 2012.

[42] JH Zheng, JJ Chen, QH Wu, and ZX Jing. Multi-objective optimization and decision making for power dispatch of a large-scale integrated energy system with distributed dhcs embedded. *Applied Energy*, 154:369–379, 2015.

[43] C. D. Korkas, S. Baldi, I. Michailidis, and E. B. Kosmatopoulos. Occupancy-based demand response and thermal comfort optimization in microgrids with renewable energy sources and energy storage. *Applied Energy*, 163:93–104, 2016.

[44] M. Hazewinkel. *Newton method, Encyclopedia of Mathematics*. Springer, 2001.

[45] Mathworks. Anti-windup control using a pid controller. `http://en.mathworks.com/help/simulink/examples/anti-windup-control-using-a-pid-controller.html`, 2016.

[46] Mathworks. fmincon. `http://en.mathworks.com/help/optim/ug/fmincon.html`, 2016.

[47] D. B. Crawley, J. W. Hand, M. Kummert, and B. T. Griffith. Contrasting the capabilities of building energy performance simulation programs. *Building and environment*, 43(4):661–673, 2008.

[48] A.P. Wemhoff. Calibration of hvac equipment pid coefficients for energy conservation. *Energy and Buildings*, 45:60–66, 2012.

[49] Qing-Guo Wang, Chang-Chieh Hang, Yong Zhang and Qiang Bi. Multivariable controller auto-tuning with its application in hvac systems. San Diego, California, 1999. Proceedings of the American Control Conference, IEEE.

[50] *Thermal Environmental Conditions for Human Occupancy.* ANSI/ASHRAE Standard 55-2013.